Acta Cryst C
STRUCTURAL CHEMISTRY

ISSN 2053-2296

Four interpenetrating hydrogen-bonded three-dimensional networks in divanillin

Marcos R. Imer,[a] Virginia Aldabalde,[b] Silvina Pagola,[c] Jacco van de Streek[d] and Leopoldo Suescun[e]*

[a]Grupo de Química Inorgánica, Departamento Estrella Campos (DEC), Facultad de Química, Universidad de la República, Av. Gral. Flores 2124, Montevideo 11800, Uruguay, [b]Grupo de Síntesis Orgánica, Departamento de Química Orgánica (DQO), Facultad de Química, Universidad de la República, Av. Gral. Flores 2124, Montevideo 11800, Uruguay, [c]Department of Chemistry & Biochemistry and COSMIC Laboratory, Old Dominion University, 4402 Elkhorn Avenue, Norfolk, VA 23529, USA, [d]Avant-garde Materials Simulation, Merzhausen, Germany, and [e]Laboratorio de Cristalografía, Química del Estado Sólido y Materiales, DETEMA, Facultad de Química, Universidad de la República, Av. Gral. Flores 2124, Montevideo 11800, Uruguay. *Correspondence e-mail: leopoldo@fq.edu.uy

Received 12 November 2018
Accepted 15 November 2018

Edited by A. L. Spek, Utrecht University, The Netherlands

Keywords: divanillin; powder diffraction; dia (Ia) topology; interpenetrating hydrogen-bond network; power diffraction; DFT-D calculation; lignin model; computational chemistry.

CCDC reference: 1879238

Supporting information: this article has supporting information at journals.iucr.org/c

The crystal structure of divainillin (systematic name: 6,6′-dihydroxy-5,5′-dimethoxy-[1,1′-biphenyl]-3,3′-dicarbaldehyde), $C_{16}H_{14}O_6$, was determined from laboratory powder X-ray diffraction data using the software *EXPO2013* (direct methods) and *WinPSSP* (direct-space approach). Divanillin molecules crystallize in the orthorhombic space group *Pba*2 (No. 32), with two molecules per unit cell ($Z' = \frac{1}{2}$). Each divanillin molecule, with twofold symmetry, is linked through strong alcohol–aldehyde hydrogen bonds to four equivalent molecules, defining a three-dimensional hydrogen-bonding network, with rings made up of six divanillin units (a diamond-like arrangement). Each molecule is also connected through π–π interactions to a translation-equivalent molecule along *c*. Four consecutive molecules stacked along [001] belong to four different three-dimensional hydrogen-bonding networks defining a quadruple array of interpenetrating networks. This complex hydrogen-bonding array is proposed as an explanation for the aging process experienced by divanillin powders.

1. Introduction

Lignin is one of the most abundant biopolymers on the earth's surface, being the main structural component of wood and some species of algae (Campbell & Sederoff, 1996; Boerjan *et al.*, 2003). Lignin's polyphenolic structure, made up of cross-linked chains of C—C- and C—O—C-bonded phenyl rings (C5—C5′ and β-O4, respectively, see Fig. 1), makes it one of the hardest to degrade natural polymers. For this reason, it plays a key role in the carbon cycle, lignin formation being one of the major natural carbon-fixation mechanisms. The production of cellulose paste (the main component of white paper), as well as the fermentation of cellulose to bio-ethanol, require the removal of lignin, making it an important hard-to-degrade residue from paper production, motivating intensive research into its possible recycling or transformation. Moreover, phenolic coupling is one of the main reactions in the biosynthesis of plants to produce secondary metabolites. This includes the synthesis of lignin from *p*-hydroxycinnamic alcohols like *p*-cumaryl alcohol, coniferyl alcohol and sinapyl alcohol (Delomenède *et al.*, 2008; Amarasekara *et al.*, 2012). Thus, toward contributing to the understanding of the structure, formation and degradation of this complex biopolymer, a series of synthetic procedures were performed to model lignin, starting from vanillin.

The first step towards obtaining a lignin analogue from vanillin is a C5—C5′ coupling, wherein divanillin is the only

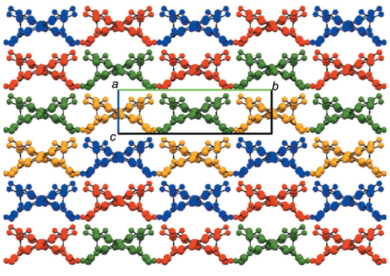

Table 1
Experimental details.

Crystal data	
Chemical formula	$C_{16}H_{14}O_6$
M_r	302.28
Crystal system, space group	Orthorhombic, *Pba*2
Temperature (K)	293
a, *b*, *c* (Å)	12.28767 (11), 13.97200 (18), 3.93043 (4)
V (Å^3)	674.79 (1)
Z	2
Radiation type	Cu $K\alpha_1$, Cu $K\alpha_2$, λ = 1.540598, 1.544426 Å
Specimen shape, size (mm)	Flat sheet, 20 × 0.5
Data collection	
Diffractometer	Rigaku ULTIMA IV
Specimen mounting	Glass sample holder with a 20 × 20 × 0.5 mm indentation for the sample
Data collection mode	Reflection, θ–θ geometry
Scan method	Step
2θ values (°)	$2\theta_{\min}$ = 4.994, $2\theta_{\max}$ = 108.104, $2\theta_{\rm step}$ = 0.01
Refinement	
R factors and goodness of fit	R_p = 0.035, R_{wp} = 0.049, $R_{\rm exp}$ = 0.022, $R(F^2)$ = 0.05040, χ^2 = 5.290
No. of parameters	116
No. of restraints	56

Computer programs: *GSAS* (Larson & Von Dreele, 2004; Toby, 2001).

product (Nishimura *et al.*, 2010). This is a very fast reaction, with the reported yield being achieved after 5 min. A longer 15 min reaction time was tested in our laboratory to improve the reaction yield. When divanillin was prepared in 5 min, a light-yellow powder, soluble in dimethyl sulfoxide (DMSO) at room temperature, was obtained, while when the reaction lasted 15 min, the light-yellow powder obtained was insoluble in DMSO. Since the chemical compositions of both powders were identical, and consistent with that of divanillin, powder X-ray diffraction (PXRD) was performed to determine whether an unexpected reaction or a polymorphic transformation were the cause for the change in solubility in the 15 min reaction product. In this report, we describe the crystal structure determination of divanillin from laboratory PXRD data of divanillin recrystallized from DMSO, using direct methods, as well as a direct-space approach. Both models were then independently refined by the Rietveld method and compared with an optimized crystal structure obtained by density functional theory (DFT) calculations. We discuss the differences encountered using both crystal structure determination methodologies and describe the complex three-dimensional arrangement of the divanillin molecules in the crystals. Furthermore, although there were no changes in the PXRD data suggesting structural or stoichiometric differences between the 5 and 15 min products, crystallite morphology changes observed by SEM suggest that the crystallite growth and consequent expansion of the hydrogen-bonding network could tentatively explain the observed solubility change.

2. Experimental

2.1. Synthesis and crystallization

Fig. 1 shows the preparation of divanillin (6,6′-dihydroxy-5,5′-dimethoxy-[1,1′-biphenyl]-3,3′-dicarbaldehyde) from vanillin (4-hydroxy-3-methoxybenzaldehyde) using horseradish peroxidase from *Armoracia rusticana* (HRPO, type VI–A, EC 1.11.1.7), as described by Nishimura *et al.* (2010), obtained as the only product in 65% yield. The full chemical path towards the preparation of lignin models can be found in Aldabalde (2015). The experiment performed under the conditions reported (5 min reaction) yielded a light-yellow powder that was separated from the solution by filtration. A small fraction of the solid was redissolved in deuterated DMSO (DMSO-d_6) and characterized by ^{1}H and ^{13}C nuclear magnetic resonance (NMR), as detailed in the supporting information. A longer 15 min reaction time was additionally tested in an attempt to improve the reaction yield. For the latter reaction time, the same yield was obtained, however the light-yellow powder obtained after filtration was insoluble in DMSO at room temperature. The product obtained as a powder showed the same elemental analysis as the expected divanillin compound, but NMR could not be used to confirm its molecular structure due to the insolubility of the solid. Later attempts to dissolve divanillin in hot DMSO [~325 (5) K] were successful, but recrystallization from this solvent or mixtures with other solvents by slow evaporation only yielded powders or very small flat needles arranged in sea-urchin-shaped balls. The needles were up to 1 mm long but less than 10 µm wide × 3 µm thick, rendering them unsuitable for single-crystal X-ray diffraction with the available instrumentation.

2.2. Powder diffraction data collection and unit-cell determination

In order to determine whether a chemical reaction or polymorphic transformation of divanillin had occurred during

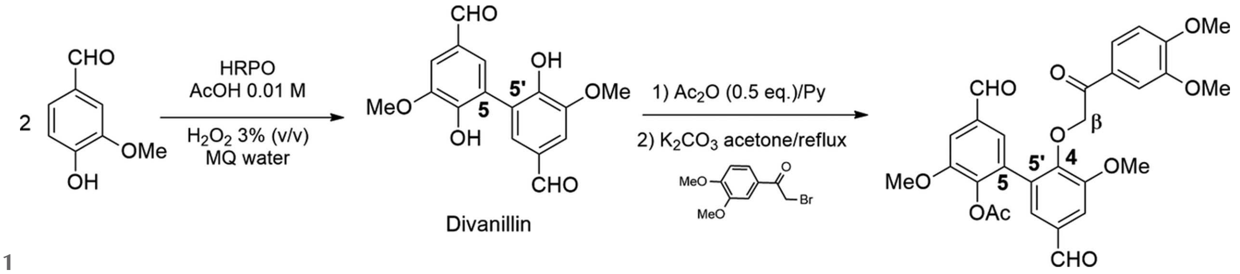

Figure 1
The preparation of divanillin from vanillin using horseradish peroxidase from *Armoracia rusticana*.

the additional 10 min of reaction time, a comparative PXRD study was performed as shown in Fig. S1 (all tables, figures and sections with the prefix 'S' are available in the supporting information). The powder diffraction patterns were identical, except for a slight difference in the absolute intensities of the peaks, suggesting improved crystallinity for the product obtained after 15 min of reaction. These PXRD patterns were also used in a search–match procedure to identify a possible impurity or unexpected solid in the reaction products. The search–match procedure using the 2013 version of the International Centre for Diffraction Data, Powder Diffraction File (PDF-2) database yielded no phases consistent with the observed powder pattern. A search for the crystal structure of divanillin or related compounds in the 2018 edition of the Cambridge Structural Database (CSD; Groom *et al.*, 2016), yielded three divanillin derivatives with the same C and O substituents in the biphenyl ring system, but also additional moieties. Moreover, a search in CAS SciFinder did not result in any crystallographic characterization of this material. A peak extraction procedure performed from the 15 min powder pattern using *Winplotr 2004* (Roisnel & Rodriguez-Carvajal, 2012) afforded 20 peaks that were indexed with *DICVOL04* (Boultif & Louër, 2004), to obtain an initial unit cell in the orthorhombic system, with a = 3.9344, b = 12.2995, c = 13.9841 Å and V = 676.707 Å^3, with figures of merit M(20) = 81.8 and F(20) = 85.5. This unit cell was confirmed by fitting the powder pattern using the Le Bail method (Le Bail *et al.*, 1988) implemented in the *GSAS*/*EXPGUI* software suite (Larson & Von Dreele, 2004; Toby, 2001) using both the 5 and the 15 min powder patterns. The confirmation of a single-phase divanillin powder, the lack of a previous crystallographic study and the impossibility of obtaining suitable single crystals for structural analysis motivated us to pursue the crystal structure determination of divanillin from powder diffraction data.

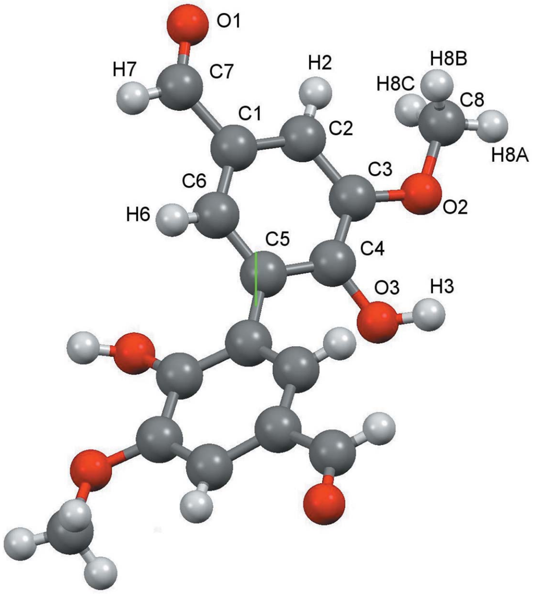

Figure 2
A divanillin molecule as obtained from the Rietveld fit. Note the atom-numbering scheme. Atoms are represented as spheres of arbitrary radii. The twofold axis between C5 and C5$^{\rm i}$ is shown as a green line. [Symmetry code: (i) $-x + 1$, $-y + 1$, z.]

Divanillin recrystallized from DMSO as a powder showed the same diffraction pattern but higher crystallinity than the original 5 and 15 min samples; therefore, a batch of this solid, thoroughly ground, was used for high-quality powder diffraction data collection using a Rigaku ULTIMA IV powder diffractometer. Data collection details are summarized in Table 1 and Section S2. Unit-cell refinement with the Le Bail method using the full high-quality pattern confirmed the previous unit cell, and the determination of systematic absences suggested the space groups *Pba*2 (No. 32) or *Pbam* (No. 55), applying the unit-cell transformation $c,-b,a$ to the above unit cell. Considering 18 Å^3 as the average atomic volume per non-H atom in organic molecules and the above unit-cell volume, an estimated value of Z = 2 was obtained. Taking into account the internal twofold symmetry of the divanillin molecules, the space group *Pba*2, with four half-molecule fragments per unit cell and $Z' = \frac{1}{2}$, was deemed most probable and crystal structure determination was first attempted using the latter space-group symmetry. Crystal data, data collection and structure refinement details are summarized in Table 1.

2.3. Crystal structure determination, Rietveld refinement and DFT-D simulation

Crystal structure determination was simultaneously attempted using direct methods implemented in the software *EXPO2013* (Altomare *et al.*, 2013) and a direct-space approach using the software *WinPSSP* (Pagola *et al.*, 2017) in the space group *Pba*2 and with $Z' = \frac{1}{2}$. The chemical formula and powder diffraction data were input into *EXPO2013*, allowing it to perform peak-search, indexing, space-group symmetry and crystal structure determination using the default calculation options. Unit-cell determination confirmed the previously indicated space group. The crystal structure determination algorithm detected the possible presence of preferential orientation effects in the pattern and successfully used this information, finding a structural model with all non-H atoms located and the expected atomic connectivity, after one run using default options and one EXTRA recycling of the initial solution. *WinPSSP* was fed with a planar model of half a divanillin molecule (one phenyl ring with –OCH$_3$, –CHO and –OH substituents) and was able to determine its position in the unit cell with enough precision to afford a correct crystal structure refinement; however, the starting model before Rietveld refinement was not as good as that from *EXPO2013*, likely due to the lack of a preferred orientation correction. Both equivalent structural models were refined to the same final model within the s.u. values reported by the Rietveld method (Loopstra & Rietveld, 1969) using the *GSAS*/*EXPGUI* suite. A linear interpolation function with 36 parameters was used to describe the background, while a pseudo-Voigt function corrected for axial divergence was used to model the profile shapes. A preferred orientation correction was also included in the Rietveld refinement using the March–Dollase model as implemented in *GSAS* to account for underestimated intensities in the *h*00 reflections. The preferred orientation ratio refined to 0.771, suggesting plate-like crystals oriented parallel to the sample surface.

Restraints for C—C, C—H, C—O and O—H bond lengths were implemented considering the connectivity of each atom in the molecule, using average bond lengths extracted from Table 9.5.1.1 of the *International Tables for Crystallography* (Vol. C, Prince, 2004). All atoms were refined with independent isotropic atomic displacement parameters, except for H atoms, which were constrained to $1.2U_{\rm iso}$ of the parent C or O atom. Fig. S2 shows the final fitted pattern and Table S1 shows the final atomic positions and isotropic atomic displacement parameters.

Furthermore, to confirm the orientation of the –OH group involved in strong hydrogen-bonding interactions that define the crystal packing, a dispersion-corrected DFT simulation (Neumann, 2017) of the crystal structure was performed (van de Streek & Neumann, 2010, 2014). The crystal structure optimizations were carried out with the software *GRACE* (Neumann, 2017), which calls *VASP* (Kresse & Joubert, 1999) for the DFT calculations. Atomic positions calculated after a three-stage optimization procedure using PBE-D3 (see Table S2) are consistent with the refined atomic coordinates, with an r.m.s. Cartesian displacement of 0.21 Å, a maximum non-H-atom displacement of 0.23 Å for atom O1 and an overall maximum displacement of 0.73 Å for atom H3, both of which are involved in the above-mentioned hydrogen bond. DFT-D results slightly improve the positions of the O3—H3 acceptor group and the O1 donor atom, therefore confirming the complex hydrogen-bonding network described in the next section. Fig. S3 shows an overlay of the models fitted from the powder diffraction data and calculated by DFT-D, wherein the difference in the O3—H3 positons are clearly visible.

3. Results and discussion

Divanillin (see Fig. 2) crystallizes in the *Pba*2 space group (No. 32), with two molecules per unit cell ($Z' = \frac{1}{2}$). The molecule displays twofold symmetry, and a crystallographic twofold axis passing through the C5—C5$^{\rm i}$ bond [symmetry code: (i) $-x + 1, -y + 1, z$] determines that only one half of the molecule is required to describe the crystal structure. The average plane of the molecule lays normal to the [001] direction, with each phenyl ring deviating by 25.28 (3)° from it (25.58° in the DFT-D model). The dihedral angle between both symmetry-equivalent phenyl rings is 129.42 (18)° (128.54° in the DFT-D model), considering the smallest angle between symmetry-equivalent groups, and is of similar magnitude to other biphenyl structures present in the CSD, where no intramolecular hydrogen bonds exist. With this molecular conformation, the hydroxy group (O3—H3) at C4 forms a strong hydrogen bond with the aldehyde group [C7—(H7)═O1] at C1 of an equivalent molecule. The geometric parameters of this hydrogen bond are given in Table 2. Due to the symmetry of the arrangement, the O3—H3···O1$^{\rm ii}$ hydrogen bond is the only one that needs to be described to explain the intermolecular connectivity. This hydrogen bond and its symmetry equivalents define a complex three-dimensional network described in the following paragraphs.

Table 2
Hydrogen-bond geometry (Å, °).

D—H···*A*	*D*—H	H···*A*	*D*···*A*	*D*—H···*A*
O3—H3···O1$^{\rm i}$	0.949 (3)	2.231 (5)	2.828 (2)	120.0 (5)

Symmetry code: (i) $-x + \frac{1}{2}, y + \frac{1}{2}, z - 1$.

When the packing of the divanillin molecules is considered, the formation of infinite chains along $[01\overline{2}]$ and $[0\overline{1}2]$, and a *C*(8) hydrogen-bonding pattern, according to Etter's notation (Etter, 1990), are observed. Each of these chains is formed by alternating coplanar phenyl rings related by a *b*-glide plane, plus an additional translation along the *c* axis, in a pattern that resembles a zipper, as shown in Fig. 3(*a*). Both chains are related by the twofold axis of the divanillin molecules; therefore, they intersect at every molecule forming the same angle as the dihedral angle between the phenyl rings; this is shown in Fig. 3(*b*). Two parallel chains with alternating divanillin molecules in one of the directions are crosslinked by two other parallel chains in the other direction, forming a six-membered ring of connected divanillin molecules, in a $R_6^6(52)$ ring pattern (see Fig. 4*a*), which is part of a three-dimensional hydrogen-bonding network obtained by interlacing both networks above. Fig. 4(*b*) shows three such $R_6^6(52)$ rings in

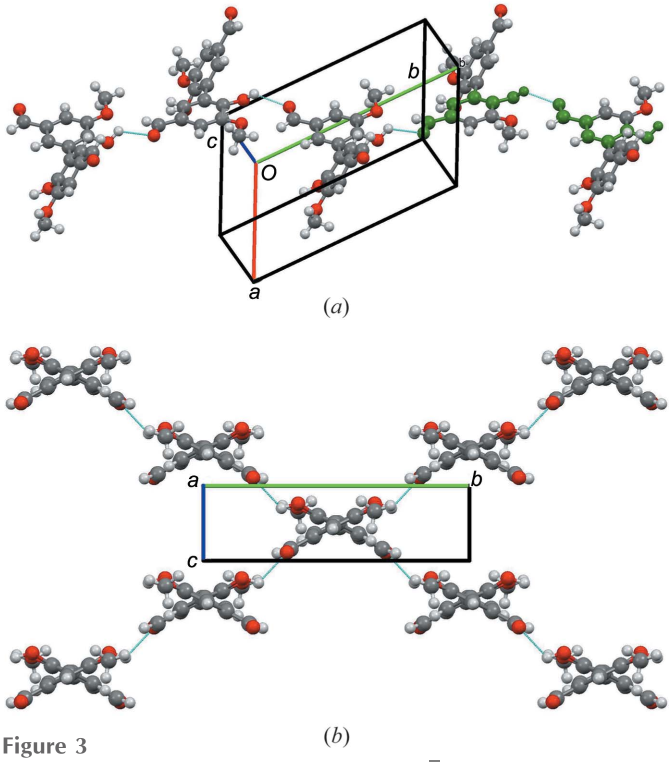

(*a*)

(*b*)

Figure 3
(*a*) Hydrogen bonding in divanillin along $[01\overline{2}]$, with the *C*(8) bonding pattern highlighted in green. (*b*) Two divanillin hydrogen-bonded chains along $01\overline{2}$ and $0\overline{1}2$, crossing at the molecule shown in the unit cell.

different orientations. Each divanillin molecule forms four hydrogen bonds (two as donor and two as acceptor) and therefore is the vertex of four such rings, in a pattern that resembles a diamond-like network. The arrangement of phenyl rings, however, defines broad rhombic windows in the network, with a 13.9 Å minimum distance between translation-equivalent atoms on both sides of the hexagonal rings. This open three-dimensional network, however, does not completely describe the structural arrangement, since divanillin molecules are closely packed together. In addition to the four hydrogen bonds mentioned above, each divanillin molecule is connected to two nearby molecules along [001] through strong π–π stacking interactions (see Fig. 5*a*). The distance between parallel phenyl-ring centroids is identical to the *c*-axis length, *i.e.* 3.9303 (3) Å (3.9289 Å), and the perpendicular ring–ring distance is 3.5541 (1) Å (3.5473 Å). These stacking interactions with the top and bottom nearby molecules define an infinite chain along [001]. The nearby [001]-translated divanillin molecule forms exactly the same hydrogen-bonding pattern as described above, but displaced by one unit cell along [001]. In an initial analysis based on growing the hydrogen-bonding network by hand, using *Mercury* (Version 3.9; Macrae *et al.*, 2008), it was apparent that two molecules along [001] were part of two independent interpenetrating networks that filled space, as shown in Fig. 5(*b*). In order to confirm this complex topology of the network, the software *ToposPro* was used (Blatov *et al.*, 2014). This not only confirmed a diamond-like network providing a standard description as a **dia** network, but also corrected the description to a four interpenetrating hydrogen-bonding network. Moreover, this packing motif consisting of four interpenetrating **dia** networks related only by translation (Ia Class) has been observed previously in 16,20-dinitro-(3,4,8,9)-dibenzo-2,7-dioxa-5,10-diaza[4,4,4]propellane (Nowicka-Scheibe *et al.*, 2003), as noted by Baburin *et al.* (2008) and described using the notation introduced by Blatov *et al.* (2004). The main difference between that compound and divanillin is the smaller size and more compact packing arrangement of the latter.

The four interpenetrating hydrogen-bonding networks and the stacking of molecules along the *c* axis – also defined by strong attractive interactions – makes this crystal packing a very stable arrangement. The disassembly of such a three-dimensional network by dissolution would require strong solvent–divanillin interactions to disrupt the intermolecular

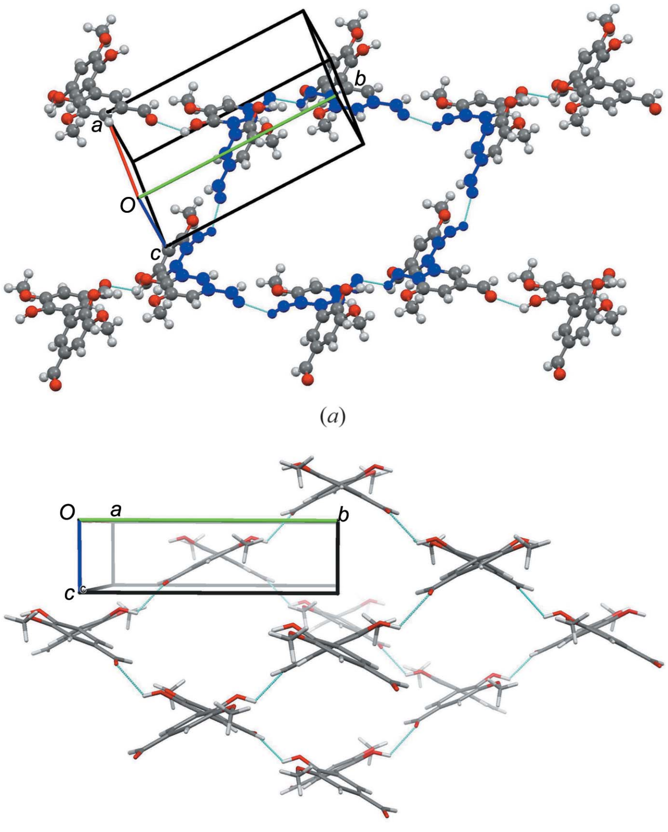

(*b*)

Figure 4
(*a*) One of the $R_6^6(52)$ rings formed by six divanillin molecules, highlighted in blue. (*b*) Three of the rings in different orientations, viewed in perspective along the *a* axis. Fainter molecules are farther away from the viewer.

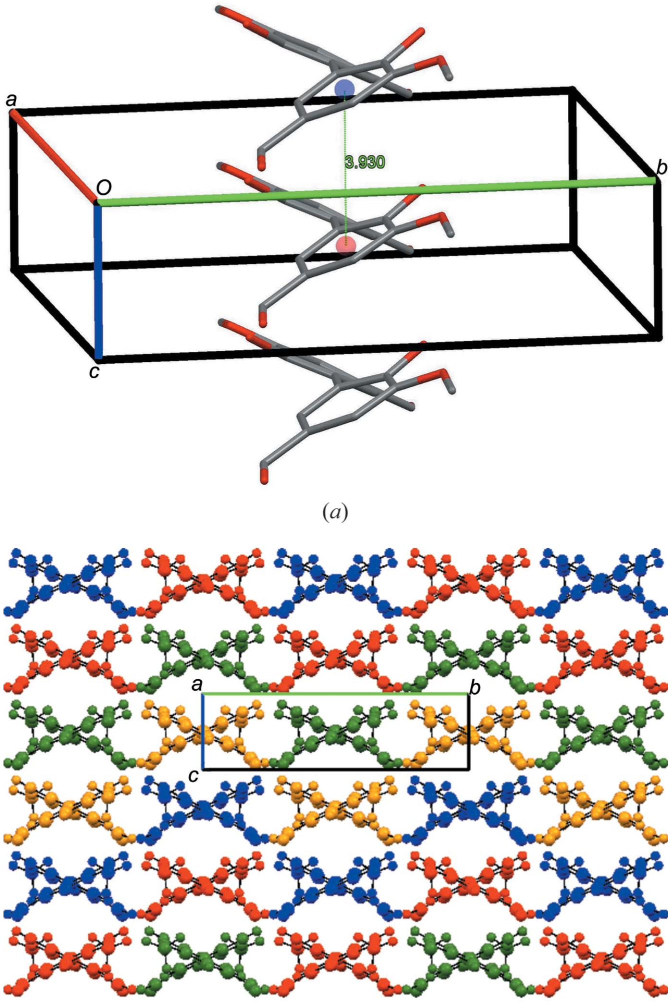

(*b*)

Figure 5
(*a*) π–π stacking interaction between translation-equivalent divanillin molecules along [001]. (*b*) The packing of four interpenetrating networks of divanillin molecules highlighted in different colours.

attractive forces in the solid and to stabilize the solvated molecules. SEM micrographs indicate that the 5 min reaction product consists of long needles; some showing curved edges, with sub-micrometre widths (see Figs. S4*a* and S4*b*). Divanillin crystals obtained after the 15 min reaction show somehow a larger plate-like shape (see Figs. S4*c* and S4*d*), consistent with the observed preferred orientation of the powder used for data collection. This morphology change, and the associated growth of the hydrogen-bonded network in the 15 min reaction product, may tentatively explain the observed solubility of the 5 min sample and the insolubility of the 15 min product in DMSO at room temperature, which initially motivated the studies presented in this article.

Acknowledgements

The authors are grateful to D. Gamenara for helpful discussions, to Magela Rodao from Servicio de Microscopía Electrónica, Facultad de Ciencias, UdelaR, for the SEM images and to L. Otero for the EA determinations.

Funding information

Funding for this research was provided by: PEDECIBA Uruguay.

References

Aldabalde, V. (2015). PhD thesis, Universidad de la República, Uruguay. http://riquim.fq.edu.uy/items/show/3182.

Altomare, A., Cuocci, C., Giacovazzo, C., Moliterni, A., Rizzi, R., Corriero, N. & Falcicchio, A. (2013). *J. Appl. Cryst.* **46**, 1231–1235.

Amarasekara, A. S., Wiredu, B. & Razzaq, A. (2012). *Green Chem.* **14**, 2395–2397.

Baburin, I. A., Blatov, V. A., Carlucci, L., Ciani, G. & Proserpio, D. M. (2008). *CrystEngComm*, **10**, 1822–1838.

Blatov, V. A., Carlucci, L., Ciani, G. & Proserpio, D. M. (2004). *CrystEngComm*, **6**, 377–395.

Blatov, V. A., Shevchenko, A. P. & Proserpio, D. M. (2014). *Cryst. Growth Des.* **14**, 3576–3586.

Boerjan, W., Ralph, J. & Baucher, M. (2003). *Annu. Rev. Plant Biol.* **54**, 519–546.

Boultif, A. & Louër, D. (2004). *J. Appl. Cryst.* **37**, 724–731.

Campbell, M. & Sederoff, R. R. (1996). *Plant. Physiol.* **110**, 3–13.

Delomenède, M., Bedos-Belval, F., Duran, H., Vindis, C., Baltas, M. & Nègre-Salvayre, A. J. (2008). *J. Med. Chem.* **51**, 3171–3181.

Etter, M. C. (1990). *Acc. Chem. Res.* **23**, 120–126.

Groom, C. R., Bruno, I. J., Lightfoot, M. P. & Ward, S. C. (2016). *Acta Cryst.* B**72**, 171–179.

Kresse, G. & Joubert, D. (1999). *Phys. Rev. B*, **59**, 1758–1775.

Larson, A. C. & Von Dreele, R. B. (2004). General Structure Analysis System (GSAS). Report LAUR 86-748. Los Alamos National Laboratory, New Mexico, USA.

Le Bail, A., Duroy, H. & Fourquet, J. L. (1988). *Mater. Res. Bull.* **23**, 447–452.

Loopstra, B. O. & Rietveld, H. M. (1969). *Acta Cryst.* B**25**, 787–791.

Macrae, C. F., Bruno, I. J., Chisholm, J. A., Edgington, P. R., McCabe, P., Pidcock, E., Rodriguez-Monge, L., Taylor, R., van de Streek, J. & Wood, P. A. (2008). *J. Appl. Cryst.* **41**, 466–470.

Neumann, M. A. (2017). *GRACE*, Version 2.4, http://www.avmatsim.eu. Avant-garde Materials Simulation SARL, France.

Nishimura, R. T., Giammanco, C. H. & Vosburg, D. A. (2010). *J. Chem. Educ.* **87**, 526–527.

Nowicka-Scheibe, J., Grech, E., Sośnicki, J. G., Głowiak, T., Sawka-Dobrowolska, W. & Sobczyk, L. (2003). *J. Mol. Struct.* **655**, 17–22.

Pagola, S., Polymeros, A. & Kourkoumelis, N. (2017). *J. Appl. Cryst.* **50**, 293–303.

Prince, E. (2004). Editor. *International Tables for Crystallography*, Vol. C, *Mathematical, Physical and Chemical Tables*. Chester: International Union of Crystallography.

Roisnel, T. & Rodriguez-Carvajal, J. (2012). *Winplotr*. http://www.cdifx.univ-rennes1.fr/winplotr/winplotr.htm.

Streek, J. van de & Neumann, M. A. (2010). *Acta Cryst.* B**66**, 544–558.

Streek, J. van de & Neumann, M. A. (2014). *Acta Cryst.* B**70**, 1020–1032.

Toby, B. H. (2001). *J. Appl. Cryst.* **34**, 210–213.

supporting information

Acta Cryst. (2018). C**74**, 1768-1773 [https://doi.org/10.1107/S2053229618016200]

Four interpenetrating hydrogen-bonded three-dimensional networks in divanillin

Marcos R. Imer, Virginia Aldabalde, Silvina Pagola, Jacco van de Streek and Leopoldo Suescun

Computing details

Program(s) used to solve structure: direct methods; program(s) used to refine structure: *GSAS*.

6,6′-Dihydroxy-5,5′-dimethoxy-[1,1′-biphenyl]-3,3′-dicarbaldehyde

Crystal data

$C_{16}H_{14}O_6$
$M_r = 302.28$
Orthorhombic, *Pba*2
Hall symbol: P 2 -2ab
$a = 12.28767\ (11)$ Å
$b = 13.97200\ (18)$ Å
$c = 3.93043\ (4)$ Å
$V = 674.79\ (1)$ Å^3
$Z = 2$
$D_x = 1.488$ Mg m^{-3}
CuKα_1, CuKα_2 radiation, $\lambda = 1.540598$, 1.544426 Å
$T = 293$ K
light yellow
flat_sheet, 20 × 0.5 mm

Data collection

Rigaku ULTIMA IV diffractometer
Radiation source: sealed X-ray tube
Curved Ge crystal monochromator
Specimen mounting: Glass sample holder with a 20x20x0.5 mm indentation for the sample
Data collection mode: reflection, θ-θ geometry
Scan method: step
$2\theta_{\min} = 4.994°$, $2\theta_{\max} = 108.104°$, $2\theta_{\text{step}} = 0.01°$

Refinement

Least-squares matrix: full
$R_p = 0.035$
$R_{wp} = 0.049$
$R_{exp} = 0.022$
$R(F^2) = 0.05040$
10312 data points
Profile function: CW Profile function number 3 with 19 terms pseudo-Voigt profile coefficients as parameterized in P. Thompson, D.E. Cox & J.B. Hastings (1987). J. Appl. Cryst.,20,79-83. Asymmetry correction of L.W. Finger, D.E. Cox & A. P. Jephcoat (1994). J. Appl. Cryst.,27,892-900. #1(GU) = 280.285 #2(GV) = -19.927 #3(GW) = 18.038 #4(GP) = 0.000 #5(LX) = 5.378 #6(LY) = 0.000 #7(S/L) = 0.0295 #8(H/L) = 0.0301 #9(trns) = 8.98 #10(shft)= 0.0000 #11(stec)= 0.00 #12(ptec)= 0.00 #13(sfec)= 0.00 #14(L11) = 0.026 #15(L22) = -0.035 #16(L33) = 2.037 #17(L12) = -0.015 #18(L13) = 0.214 #19(L23) = -0.135 Peak tails are ignored where the intensity is below 0.0010 times the peak Aniso. broadening axis 0.0 0.0 1.0
116 parameters
56 restraints
H-atom parameters not defined?

$(\Delta/\sigma)_{\max} = 0.02$

Background function: GSAS Background function number 7 with 36 terms. Linear interpolation 1: 746.117 2: 636.840 3: 820.260 4: 1087.66 5: 1340.36 6: 1694.77 7: 1939.95 8: 1780.04 9: 1470.80 10: 1469.09 11: 1171.58 12: 1220.23 13: 1099.08 14: 1133.77 15: 1082.14 16: 1040.03 17: 920.035 18: 960.677 19: 942.495 20: 867.667 21: 833.747 22: 817.667 23: 803.239 24: 778.713 25: 734.737 26: 743.098 27: 717.039 28: 697.800 29: 637.240 30: 613.791 31: 574.878 32: 571.899 33: 544.400 34: 538.892 35: 514.075 36: 523.654

Preferred orientation correction: March-Dollase AXIS 1 Ratio= 0.77078 h= 1.000 k= 0.000 l= 0.000 Prefered orientation correction range: Min= 0.67671, Max= 2.18374

Fractional atomic coordinates and isotropic or equivalent isotropic displacement parameters (Å²)

	x	*y*	*z*	$U_{\rm iso}$*/$U_{\rm eq}$
O1	0.13485 (8)	0.31375 (11)	0.8931 (7)	0.0784 (8)*
O2	0.20440 (9)	0.64551 (12)	0.2917 (7)	0.0663 (8)*
O3	0.42399 (10)	0.64420 (7)	0.2402 (5)	0.0707 (7)*
C1	0.27806 (12)	0.41290 (11)	0.6785 (6)	0.0470 (13)*
C2	0.21080 (10)	0.48780 (17)	0.5520 (9)	0.0493 (11)*
C3	0.26177 (13)	0.56830 (16)	0.4107 (11)	0.0598 (13)*
C4	0.37574 (11)	0.57070 (11)	0.4036 (6)	0.0607 (14)*
C5	0.44038 (11)	0.49460 (17)	0.5	0.0375 (12)*
C6	0.38971 (11)	0.41765 (11)	0.6453 (6)	0.0532 (13)*
C7	0.23099 (9)	0.32760 (9)	0.8444 (6)	0.0808 (14)*
C8	0.08772 (11)	0.64343 (8)	0.3383 (3)	0.0567 (9)*
H2	0.13565 (13)	0.4859 (6)	0.579 (2)	0.0592 (13)*
H3	0.4013 (4)	0.70692 (13)	0.2997 (15)	0.0848 (9)*
H6	0.4332 (2)	0.37013 (16)	0.7397 (10)	0.0638 (15)*
H7	0.2795 (2)	0.27727 (16)	0.9036 (16)	0.0969 (16)*
H8A	0.0593 (3)	0.70318 (13)	0.2656 (12)	0.0681 (11)*
H8B	0.0718 (4)	0.6328 (5)	0.5720 (4)	0.0681 (11)*
H8C	0.0553 (3)	0.59394 (16)	0.2069 (7)	0.0681 (11)*

Geometric parameters (Å, º)

C3—C2	1.402 (4)	C7—C1	1.477 (2)
C3—C4	1.401 (2)	C7—O1	1.2124 (16)
C3—O2	1.371 (3)	C7—H7	0.951 (3)
C2—C3	1.402 (4)	O1—C7	1.2124 (16)
C2—C1	1.423 (3)	C8—O2	1.4456 (18)
C2—H2	0.930 (2)	C8—H8A	0.949 (3)
C1—C2	1.423 (3)	C8—H8B	0.951 (3)
C1—C6	1.380 (2)	C8—H8C	0.951 (3)
C1—C7	1.477 (2)	H6—C6	0.929 (3)
C6—C1	1.380 (2)	H2—C2	0.930 (2)

C6—C5	1.367 (3)	H8A—C8	0.949 (3)
C6—H6	0.929 (3)	H8A—H8B	1.562 (6)
C5—C6	1.367 (3)	H8A—H8C	1.545 (3)
C5—C5^{i}	1.473 (3)	H8B—C8	0.951 (3)
C5—C4	1.380 (3)	H8B—H8A	1.562 (6)
C4—C3	1.401 (2)	H8B—H8C	1.548 (4)
C4—C5	1.380 (3)	H8C—C8	0.951 (3)
C4—O3	1.349 (2)	H8C—H8A	1.545 (3)
O3—C4	1.349 (2)	H8C—H8B	1.548 (4)
O3—H3	0.949 (3)	H7—C7	0.951 (3)
O2—C3	1.371 (3)	H3—O3	0.949 (3)
O2—C8	1.4456 (18)		
C2—C3—C4	118.3 (2)	C3—C4—C5	123.45 (17)
C2—C3—O2	122.46 (15)	C3—C4—O3	117.85 (18)
C4—C3—O2	119.2 (2)	C5—C4—O3	117.67 (13)
C3—C2—C1	117.96 (13)	C4—O3—H3	117.2 (3)
C3—C2—H2	120.7 (5)	C3—O2—C8	116.80 (16)
C1—C2—H2	121.1 (6)	C1—C7—O1	125.47 (15)
C2—C1—C6	120.60 (16)	C1—C7—H7	117.4 (2)
C2—C1—C7	121.35 (13)	O1—C7—H7	117.0 (2)
C6—C1—C7	118.04 (14)	O2—C8—H8A	108.0 (3)
C1—C6—C5	122.01 (15)	O2—C8—H8B	109.2 (4)
C1—C6—H6	119.9 (2)	O2—C8—H8C	111.2 (3)
C5—C6—H6	117.9 (2)	H8A—C8—H8B	110.6 (5)
C6—C5—C5^{i}	122.2 (2)	H8A—C8—H8C	108.8 (3)
C6—C5—C4	117.29 (13)	H8B—C8—H8C	109.0 (4)
C5^{i}—C5—C4	119.6 (2)		

Symmetry code: (i) $-x+1, -y+1, z$.

Hydrogen-bond geometry (Å, º)

D—H···*A*	*D*—H	H···*A*	*D*···*A*	*D*—H···*A*
O3—H3···O1^{ii}	0.949 (3)	2.231 (5)	2.828 (2)	120.0 (5)

Symmetry code: (ii) $-x+1/2, y+1/2, z-1$.